Solution structure of calcium-free calmodulin

Hitoshi Kuboniwa [1], Nico Tjandra [1], Stephan Grzesiek [1], Hao Ren[2], Claude B. Klee[2], and Ad Bax[1]

The three-dimensional structure of calmodulin in the absence of Ca^{2+} has been determined by three- and four-dimensional heteronuclear NMR experiments, including ROE, isotope-filtering combined with reverse labelling, and measurement of more than 700 three-bond *J*-couplings. In analogy with the Ca^{2+}-ligated state of this protein, it consists of two small globular domains separated by a flexible linker, with no stable, direct contacts between the two domains. In the absence of Ca^{2+}, the four helices in each of the two globular domains form a highly twisted bundle, capped by a short anti-parallel β-sheet. This arrangement is qualitatively similar to that observed in the crystal structure of the Ca^{2+}-free N-terminal domain of troponin C.

[1]Laboratory of Chemical Physics, National Institute of Diabetes and Digestive and Kidney Diseases, and [2]Laboratory of Biochemistry, National Cancer Institute, National Institutes of Health, Bethesda, Maryland 20892-0520, USA

Correspondence should be addressed to A.B.

Calmodulin is a ubiquitous intracellular protein of 148 residues (M_r 16,700) that plays a critical role in coupling transient Ca^{2+} influx, caused by a stimulus at the cell surface, to events in the cytosol[1]. It performs this role by binding to a host of intracellular enzymes in a calcium-dependent manner. The X-ray crystal structure of Ca^{2+}-ligated calmodulin resembles a dumbbell, in which the small globular amino- and carboxy-terminal domains are linked by a 26-residue α-helix, frequently referred to as the 'central helix'[2]. ^{15}N NMR relaxation experiments[3] and small-angle X-ray scattering studies[4] indicate that this helical linker is highly flexible in solution. However, NMR data also indicate that the structures of the globular domains of Ca^{2+}-ligated calmodulin in solution are very similar to those observed in the crystalline state[5,6]. Each domain consists of a pair of helix-'loop'-helix motifs, which are commonly called 'EF-hands'[7]. The 'loops' of these two EF-hands are linked by a short antiparallel β-sheet. Attempts to grow apo-calmodulin crystals suitable for X-ray studies have failed, but a detailed model for its structure has been put forward based on the highly homologous (51% sequence identity) protein troponin C (ref. 8). In the X-ray structure of troponin-C (ref. 9), the two EF-hands in the C-terminal domain are both ligated to Ca^{2+}, whereas the EF-hands in the N-terminal domain are not. Although the folds of the apo and Ca^{2+}-ligated domains are similar, a large difference in the relative orientations of the four α-helices is observed, which results in the formation of a pronounced hydrophobic pocket between the four helices in the Ca^{2+}-ligated state. Herzberg *et al.*[10] proposed that this conformational difference constitutes the basis for 'activating' Ca^{2+}-modulated EF-hand proteins. The NMR and X-ray structures for complexes between calmodulin and two myosin light chain kinase peptide fragments confirmed that the hydrophobic pockets play an important structural role in the binding of calmodulin to its target enzymes[11,12].

The EF-hand motif is found in a wide range of Ca^{2+}-binding proteins with very diverse functions. Structural information for most of these proteins is only available in the Ca^{2+}-ligated state or, as was the case for the N-terminal domain of troponin C, in the apo form. A recent solution NMR study of calbindin D_{9k} was the first to directly compare the structures of the same protein in both the Ca^{2+}-free and Ca^{2+}-ligated states[13]. Although calbindin D_{9k} has significant sequence homology with calmodulin, no large rearrangement of the α-helices was observed for this protein upon metal binding. This deviation from what the Herzberg model[10] predicted was ascribed to the function of calbindin D_{9k}, which has a Ca^{2+}-buffering role rather than a regulatory one. A preliminary NMR study of the Ca^{2+}-ligated N-terminal domain of troponin C (ref. 14) supports the Herzberg conformational switch model. A preliminary report on the solution structure of the C-terminal domain of calmodulin[15] also provides qualitative support for the Herzberg model and for the apo calmodulin model of Strynadka and James. However, a recent study of the rotational dynamics of apo-calmodulin showed a difference in the ^{15}N NMR relaxation times of helices C and D, attributed to motional anisotropy, that appeared incompatible with the nearly antiparallel orientation of helices C and D reported for the model structure.[16]

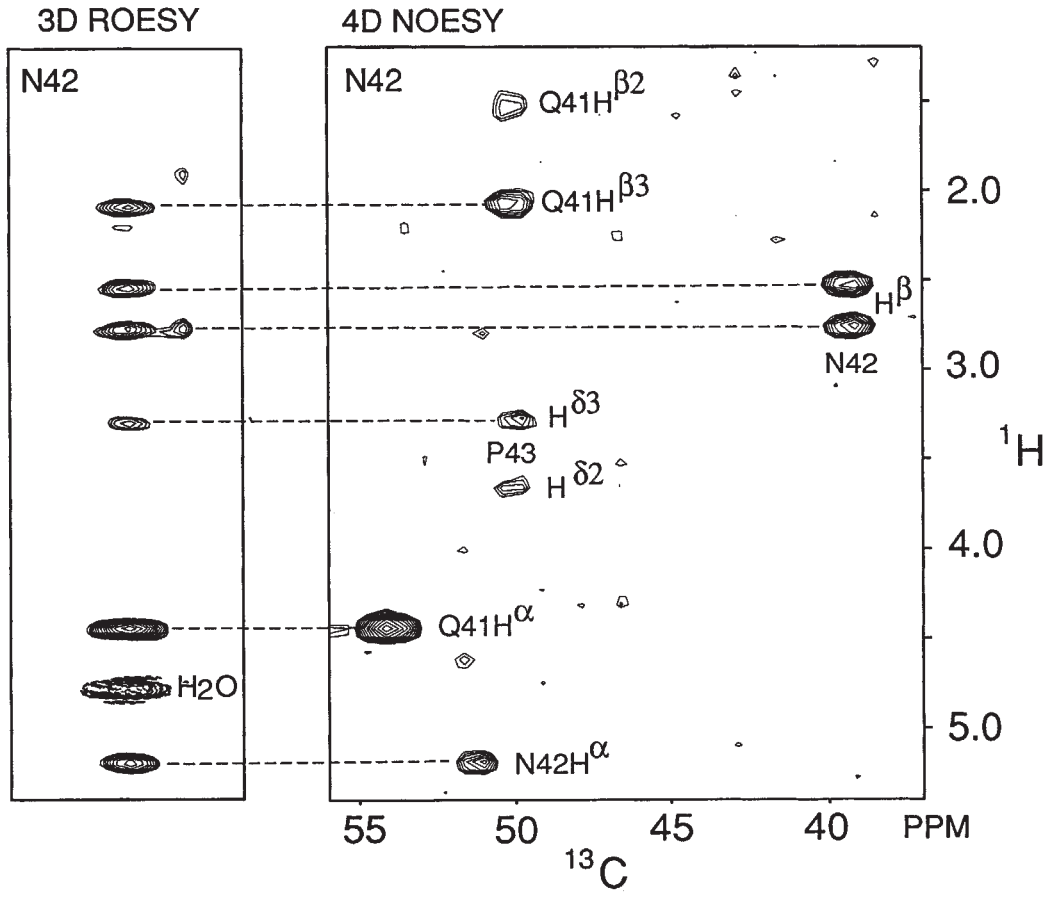

Fig. 1 Comparison of a strip taken from the 3D ^{15}N-separated ROESY spectrum (25 ms) with the corresponding cross-section from the 4D ^{13}C/^{15}N separated NOESY spectrum (80 ms), showing interactions to the amide proton of Asn 42. Cross-peaks present in NOESY but not in ROESY are dominated by spin diffusion. A cross-peak at the H_2O frequency in the ROESY strip is of opposite sign (dashed contours) and results from hydrogen exchange of the Asn 42 back-bone amide proton with the solvent.

Here we present the three-dimensional structure of apo calmodulin as determined by modern multi-dimensional NMR techniques, which permits a detailed study of the conformational changes that take place upon calcium binding. Many of the techniques and procedures used in the structure determination process are relatively new, and the experimental aspects of this study will therefore be emphasized, whereas a detailed description and an evaluation of the importance of the individual experiments for the quality of the final structure will be presented elsewhere.

Structural information from *J*-couplings

As with interproton distance constraints obtained from NOEs, dihedral constraints obtained from *J*-couplings contain important information for calculating the structure of a protein in solution. The sample of apo-calmodulin was enriched uniformly in ^{13}C and ^{15}N and has been used in our laboratory for the development of numerous new techniques for measuring *J*-couplings. As a consequence, a large number of three-bond *J*-couplings (over 700) was measured for apo calmodulin, covering a wide range of different types. For example, three-bond *J*-couplings between aliphatic carbons were measured[17] and indicated that all eight Ile residues have a χ_2 angle of 180°. This permitted stereospecific assignments of the H^{γ} methylene protons to be made, based on the large *J*-coupling between the $C^{\gamma 2}$ methyl carbon and $H^{\gamma 13}$, and on the strong NOE between the $C^{\gamma 2}$ methyl protons and $H^{\gamma 12}$. For two of these Ile residues (Ile 63 and Ile 130), *J*-couplings between the C^{γ} methyl carbon and the back-bone carbonyl and ^{15}N indicate that the χ_1 angle is subject to conformational averaging. These conclusions are confirmed by strong rotating frame Overhauser effects (ROEs) between the back-bone amides of these residues to H^{β} and both $H^{\gamma 12}$ and $H^{\gamma 13}$ methylene protons. No physically reasonable conformation of the side chain can simultaneously satisfy these short distances and, as confirmed by measurement of H^{α}–H^{β}, $C^{\gamma 2}$–N, and $C^{\gamma 2}$–C' couplings, the χ_1 angle of these two Ile residues is subject to rotamer averaging. On the basis of ^{13}C–^{13}C and ^{13}C–^{15}N *J*-couplings, the same conclusion could be drawn about the χ_1 angle of Val 55. Remarkably, the H^{α}–H^{β} *J*-coupling for this residue is found to be large (~10 Hz), which would normally be taken as an indication of a *trans* *J*-coupling, or a χ_1 angle of 180°. A similarly large H^{α}–H^{β} *J*-coupling is expected for the energetically unfavorable χ_1=0° rotamer, however. Based on the *J*-couplings and virtually identical patterns of both short- and long-range NOEs to the two Val 55 methyl groups, we conclude that the χ_1 angle of this residue rapidly fluctuates between 0° and 180°, with both states approximately equally populated. In commonly used force-field parametrizations used for molecular dynamics calculations, population of the $\chi_1 \approx 0°$ angle is energetically costly (~3 kcal mol^{-1}). This suggests that Val 55 destabilizes the structure in this region of the protein, possibly for lowering the height of the energy barrier involved in the structural transition from the apo to the Ca^{2+}-ligated state.

Interproton distance measurement from ROE

Measurement of the back-bone ^{15}N amide relaxation times indicates that the overall motion of the protein is not quite isotropic but, on average, is described by a rotational correlation time, τ_c, of ~8 ns (ref. 16). For such a relatively long τ_c value, NOE cross-peaks build up rapidly and indirect NOE effects (spin diffusion) can be a significant problem, making the NOE-derived distances appear shorter than their true values. In contrast to NOEs, ROEs are positive and increase monotonically with τ_c, and indirect effects are opposite in sign relative to direct effects[18,19]. For a ROE mixing time that is about 20% shorter than the average spin-locked transverse relaxation time, $T_{1\rho}$, which is close to optimal with respect to sensitivity, indirect ROE effects tend to be quite small. In practice, the indirect ROE contribution to a cross peak decreases the direct ROE and results in an overestimate of the true distance. When using upper-limit distance constraints, such an overestimate of the distance merely loosens the constraint imposed on the structure, and does not force hydrogens to be more proximate than their true value.

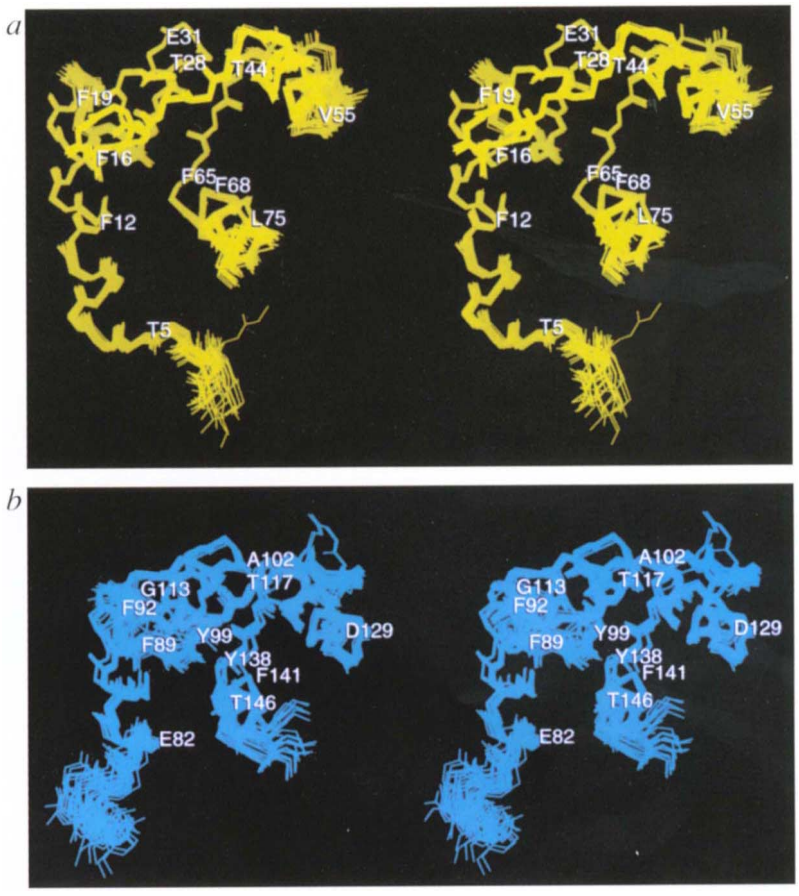

Fig. 2 Stereo view of the back-bone superposition of the 25 lowest energy conformers of *a*, the N-terminal and *b*, the C-terminal domain of apocalmodulin. To provide an indication of the peptide plane orientation, the back-bone carbonyl oxygens have been included.

Fig. 1 compares a cross-section through the four-dimensional (4D) NOESY spectrum with the equivalent cross-section taken through the three-dimensional (3D) ROESY spectrum. Both panels show the protons that are in close proximity to the back-bone amide of Asn 42. The 4D spectrum is invaluable as it provides not only the ^1H shift of the second site, but also that of the directly attached ^{13}C, allowing for a more unambiguous identification of these protons than could be made on the basis of their ^1H shift alone. Comparison with the corresponding section of the 3D ROESY spectrum shows, however, that the interactions to Gln 41 $H^{\beta 2}$ and Pro 43 $H^{\delta 2}$ are dominated by indirect effects, and the corresponding distance constraints have not been used in the structure calculation. The Asn 42 amide also shows a strong positive cross-peak with water which is opposite in sign to the true ROE cross-peaks and is caused by rapid hydrogen exchange. Although a number of other back-bone amides exhibit negative ROE cross-peaks to water, all of these can be explained by the proximity of the back-bone amide protons to rapidly exchanging hydroxyl protons of Ser and Thr residues. Thus, we have found no evidence for tightly bound water molecules in the proximity of back-bone amides

Reverse labelling of Phe residues

Besides determining the correct local geometry, which in our case is based primarily on the measurement of *J*-couplings and ROEs, identification of NOEs between residues that are far apart in the primary sequence is critical to determining as accurate a structure as possible. Such interactions are found primarily between hydrophobic residues in the core of the protein. We have used regular 4D $^{13}C/^{13}C$-separated NOESY for identifying interactions between aliphatic side chains, but as pointed out previously, this type of experiment provides less than optimal resolution when studying interactions involving Phe residues[20]. NOEs to these residues are studied most conveniently using a reverse labelling procedure, where Phe residues are at natural abundance and the rest of the protein is enriched in ^{13}C (ref. 21). This allows the interactions with these residues to be studied at high resolution and high sensitivity. The eight Phe residues in calmodulin provided nearly 200 long range NOE constraints, or about 50% of the total number of long-range constraints. Resonance assignments of the Phe aromatic ring protons were made using a combination of homonuclear ^1H isotropic mixing experiments and a ^{12}C-filtered NOESY to correlate H^{δ} to the H^{β} and H^{α}

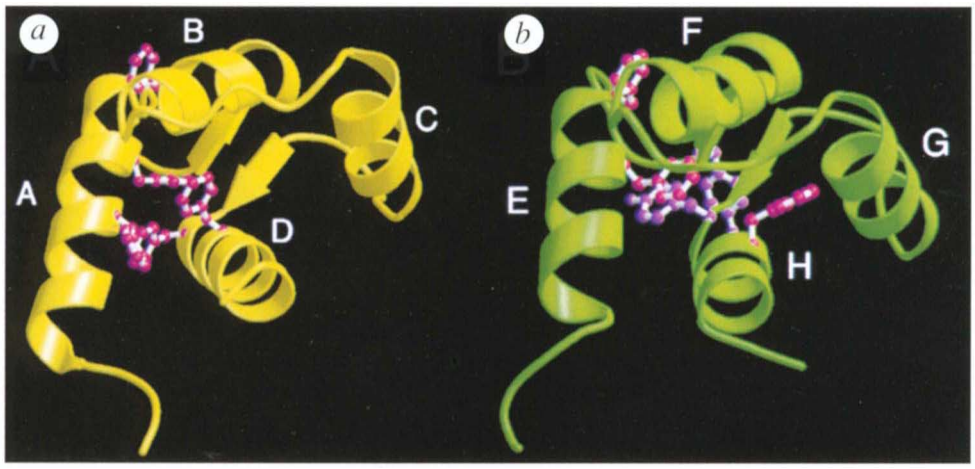

Fig. 3 MOLSCRIPT[39] stereo diagrams of *a*, the N-terminal domain and *b*, the C-terminal domain of apo calmodulin. Phe side chains (red) and Tyr side chains (magenta) are also shown. The domains are connected by a flexible linker (Met 76 through Ser 81) and their relative orientation is ill-determined.

resonances[21]. The H^{β} and H^{α} resonances were assigned based on standard triple-resonance experiments using a sample uniformly enriched with ^{13}C and ^{15}N.

Back-bone dynamics

As reported previously[16], the secondary structure of apo calmodulin is very similar to that observed in the Ca^{2+}-ligated state. Hydrogen exchange measurements indicate, however, that the hydrogen bonding network in apo-calmodulin is considerably less stable, particularly in the C-terminal domain where all amides exchange with solvent in less than ~15 minutes[16]. In the first halves of the 'loop' regions of the four helix-'loop'-helix calcium binding sites, rapid amide-hydrogen exchange is observed and ^{15}N relaxation parameters indicate higher-than-average amplitudes for the rapid internal motions of the back bone atoms[16]. These more flexible loop regions each contain three residues that ligate Ca^{2+} in the X-ray structure, so their increased disorder in the absence of Ca^{2+} is not surprising. In this respect, it is interesting to note that in the homologous protein calbindin D_{9k}, the canonical Ca^{2+}-binding loop also shows an increase in back-bone dynamics in the absence of Ca^{2+}, whereas the other Ca^{2+}-binding site, which is part of a so-called 'pseudo-EF-hand', does not[22]. In apo calmodulin, the short β-strand and the first turn of the following helix (which constitute the second half of the Ca^{2+}-binding 'loop' and contain the three remaining protein-calcium coordination sites) do not show any pronounced increase in the back-bone dynamics.

As was found previously for Ca^{2+}-ligated calmodulin in solution[3], the C-terminal helix of the N-terminal globular domain (helix D) is connected to the first helix of the C-terminal domain (helix E) by a flexible linker, extending from Met 76 to Ser 81. This contrasts with the crystalline state of Ca^{2+}-ligated calmodulin, where this linker is ordered and an integral part of the so-called 'central helix'[2]. The $^{13}C^{\alpha}$ chemical shifts for Met 76 to Ser 81 in apo calmodulin are ~1 p.p.m. downfield from their random-coil values, and strong sequential NOE connectivities between the H^{α} of residue *i* and the amide proton of residue *i*+1 indicate that the linker adopts an extended conformation for a significant fraction of the time. However, it is also interesting to note that, in contrast to Ca^{2+}-ligated calmodulin, weak NOE connectivities between the H^{α} of residue *i* and the amide of residue *i*+3 are observed all the way up to the H^{N} proton of Asp 80, suggesting that this region also adopts a helical conformation for a significant fraction of the time[22]. Based on $^{3}J_{HNH\alpha}$ values that are closer to random-coil values than to what is expected for an α-helix, and deviations from random coil $^{13}C^{\alpha}$ shifts that are about threefold smaller than observed in an α-helix, we estimate that the Met 76 to Ser 81 linker adopts a helical conformation for about one- third of the time. Considering the presence of observable $d_{\alpha N}(i,i+3)$ NOE connectivities, this helical conformation must be relatively long lived—at least several ns. The H^{α} protons of Thr 79 and Asp 80 show weak NOE (*i*, *i*+2) connectivities to the amide protons of Ser 81 and Glu 82, but no (*i*, *i*+3) connectivities, suggesting that this region may adopt transiently a 3_{10} conformation. It is interesting to note that in the Ca^{2+}-ligated state there is no direct NMR evidence for the transient presence of a helical conformation in this region of the polypeptide, even though an α-helical conformation is observed in the X-ray structure of Ca^{2+}-calmodulin[2]. The significantly larger degree of rotational diffusion anisotropy observed for apo

Table 1 Interhelical angles in calmodulin[1]

	apo CaM	model[3]	Ca^{2+}-CaM[4]
A/B[2]	138±2	134	87
A/C	88±3	90	160
A/D	127±2	119	110
B/C	126±3	130	113
B/D	47±2	45	45
C/D	130±3	141	84
E/F	131±4	137	105
E/G	81±5	84	142
E/H	142±5	119	119
F/G	141±5	131	113
F/H	30±5	47	37
G/H	133±4	146	96

[1]The axis orientation for an α-helix consisting of *K* residues is calculated by averaging the positions of 10 consecutive back-bone atoms, starting with the N atom of residue 1 through the N of residue 4, and connecting this average position to the average atom position of 10 atoms starting at the C' of residue *K*-3.
[2]Helices are defined as follows: A (6–18), B (29–38), C (45–54), D (65–74), E (83–91), F (102–111), G (118–127), H (139–145).
[3]Based on the model of Strynadka and James[8]. Coordinates were kindly provided by N. Strynadka.
[4]From ref. 2.

calmodulin[16] relative to Ca^{2+}–calmodulin[3] supports the conclusion that the linker has more of a helical character in the apo state compared to the Ca^{2+}-ligated state of the protein. Qualitatively, this also agrees with trypsin digestion experiments, which indicated a higher sensitivity to proteolysis at Lys 77 in the Ca^{2+}-ligated state[24].

No NOEs are observed between residues in the N-terminal domain and residues in the C-terminal domain, confirming that in solution, apo calmodulin also exists as two small globular domains, connected by a flexible tether which transiently adopts a helical conformation. The precision at which the structure of the C-terminal domain can be determined is severely limited by conformational averaging processes that take place on a microsecond to millisecond time scale (*vide infra*). The N-terminal domain is not affected by such averaging and its structure has been determined at high resolution. We therefore first discuss this N-terminal domain, as it provides the clearest picture of a calmodulin EF-hand pair in the absence of calcium.

Structure of the N-terminal domain

Fig. 2*a* shows a superposition of the back bones of the 25 lowest energy structures for the N-terminal domain. The r.m.s.d. relative to the mean of the non-hydrogen atom positions for residues 5 through 75 is 0.35 Å for the back-bone and 0.71 Å for all non-hydrogen atoms. There are no consistent NOE violations larger than 0.15 Å, except for the flexible N-terminal residues and the side chains of Val 55 and Ile 63, for which *J*-couplings indicate that χ_1 rotamer averaging is taking place. A ribbon diagram showing the structure of the N-terminal domain of apo calmodulin is shown in Fig. 3*a*. Thr 5 forms the N-cap residue of helix A, and continues through Leu 18. The presence of an N-cap is identified by the characteristic $^{13}C^{\alpha}$ and $^{13}C^{\beta}$ chemical shifts of the N-cap residue[24], *i*, and by a $d_{N\beta}(i,i+3)$ NOE. In addition, for all six N-caps identified in apo calmodulin NOEs are observed between the hydrophobic side chains of residues *i*-1 and *i*+4, which are predicted to have a hydrophobic interaction[25].

Phe 19 and Asp 20 form 3_{10}-type hydrogen bonds to Phe 16 and Ser 17, respectively. The region from Lys 21 through Gly 25 shows an increase in back-bone dynamics[16] and starts with a γ turn. The short β-strand (Thr 26 through Thr 28) is well-ordered and immediately precedes helix B, which starts with an N-cap at Thr 28. Helix B has a pronounced kink at residue 31, which is partly responsible for the large change in the orientation of this helix relative to Ca^{2+}-ligated calmodulin (Table 1). Helix C starts with an N-cap at Thr 44 and continues through Glu 54 as an α-helix, and in most of the NMR structures Val 55 and Asp 56 also form α-helical hydrogen bonds. Residues Ala 57 through Gly 61 are dynamically disordered and precede the well-defined second β-strand (Thr 62–Asp 64). Helix D initiates at Phe 65 and continues as a regular α-helix through Lys 75, although a proline residue at position 66 induces a small kink near the start of this helix. The orientation of the second β-strand relative to helix D is similar to what is found in Ca^{2+}-ligated calmodulin[2], but the C/D interhelix angle is very different (Table 1).

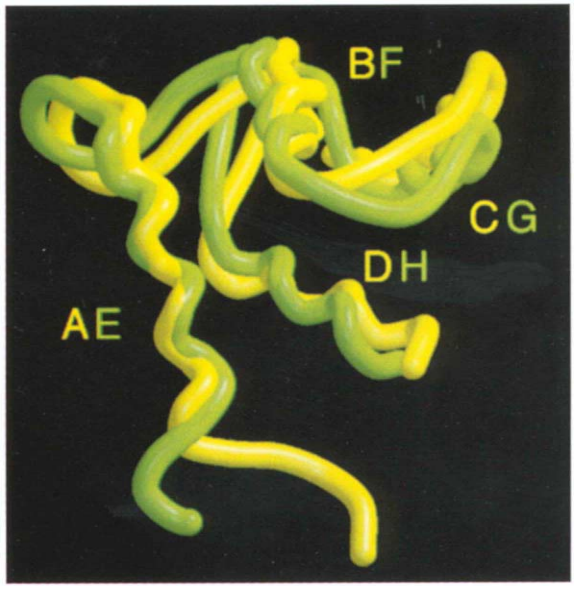

Fig. 4 Comparison of the back-bone conformation of the N- (yellow) and C-terminal (green) domains of apo calmodulin.

Structure of the C-terminal domain

As mentioned above, the structure of the C-terminal domain cannot be determined at the same level of precision as the N-terminal domain due to the presence of a conformational exchange process that takes place on an intermediate time scale of several hundred microseconds (ref. 16). However, it was estimated from ^{15}N relaxation measurements that one of the two conformers has a low population (5–10%), and this minor conformer is therefore not expected to contribute much to strong NOE interactions in this domain. In addition to this relatively slow exchange process, homo- and heteronuclear *J*-couplings indicate rapid conformational averaging for the side chains of many of the hydrophobic residues in this domain.

The first helix of the C-terminal domain (helix E) becomes well defined starting at Glu 82 and extends to Val 91 (Fig. 3*b*). Rapid χ_1 rotamer averaging of Val 91 is inconsistent with an α-helical hydrogen bond from Phe 92 to Ala 88, and structure calculations confirm the absence of this hydrogen bond. Instead, in most of the

Table 2 Comparison of α-helical back bone atom positions[1]

	apo CaM-N	apo CaM-C	model-N[2]	model-C[2]	Ca^{2+}–CaM-N
apo CaM-C	2.01				
model-N[2]	1.06	2.01			
model-C[2]	1.09	1.99	0.34		
Ca^{2+}–CaM-N	3.91	3.84	3.95	3.70	
Ca^{2+}–CaM-C	3.01	3.30	3.09	3.14	0.75

[1]r.m.s differences (Å), using the definitions of the helices given in the footnote to Table 1, except when comparing helices from the N- and C-terminal domains, where the shorter of the pair of homologous helices is used to define the residues. Domains are superimposed using the back-bone atom positions of the four helices.
[2]models are from ref. 8.

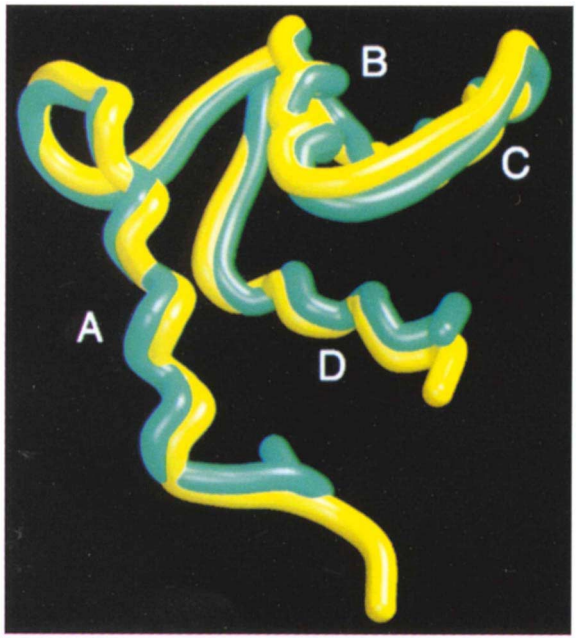

Fig. 5 Comparison of the backbone conformation of the N-terminal domain of the apo calmodulin NMR structure (yellow) with the model of Strynadka and James[8] (blue).

structures Phe 92 and Asp 93 make 3_{10} hydrogen bonds to Phe 89 and Arg 90, analogous to the 3_{10} hydrogen bonds observed for Phe 19 and Asp 20 in the N-terminal domain. The first part of the Ca^{2+} binding 'loop', following helix E, is poorly defined by the NOE data and dynamically disordered based on ^{15}N relaxation data. In the Ca^{2+}-ligated X-ray structure, Phe 99 to Ser 101 form a short antiparallel β-sheet with Gln 135 to Asn 137. NOEs characteristic for this short antiparallel β-sheet are also observed in apo calmodulin, including H^{α}–H^{α} NOEs between Tyr 99 and Asn 137 and between Ser 101 and Gln 135, an H^{N}–H^{N} NOE between Tyr 99 and Val 136, and a H^{N}–H^{α} NOE between Ala 102 and Gln 135. The sheet is strongly twisted and the two hydrogen bonds between Ile 100 and Val 136 are the only ones present in the majority of the calculated structures. Helix F starts with an N-cap at Ser 101 and continues through Leu 112. This helix does not exhibit the distinct kink observed at residue Glu 31 for the homologous helix in the N-terminal domain, but the more pronounced twist observed in the β-sheet partly makes up for the absence of the kink. This results in an E/F interhelix angle which is not much smaller than that between helices A and B (Table 1). Residues Gly 113 through Leu 116 form a rather flexible but extended solvent-exposed loop, connecting helices F and G. Helix G starts with an N-cap at Thr 117 and continues to Glu 127. Residues Asn 129 through Gly 134, preceding the second β-strand, are poorly defined by the NMR data due to extensive line broadening caused by conformational averaging in this region of the structure. The last helix, H, which begins at Tyr 138 in the Ca^{2+}-ligated state, appears to initiate at Glu 139. In contrast to the Ca^{2+}-ligated state, no characteristic N-cap conformation at the start of this helix is seen. The back-bone angles of Thr 146 through Lys 148 are dynamically disordered.

Comparison of N- and C-terminal domains

Comparison of the best-fit superpositions of the α-helices of the N- and C-terminal domains shows rather similar structures for the two domains in the apo state (Fig. 4). However, this structural similarity is less than what was previously observed in the Ca^{2+}-ligated state (Table 2). In part, the larger difference between the structure of the two domains in the apo state might be attributed to the relatively low precision of the C-domain solution structure. However, there are also a number of significant structural differences that fall well outside the range of uncertainty. One example is the absence of the pronounced kink in helix F, but its presence in helix B. Another example is the interaction between the aromatic ring of Phe 141 and back-bone and side-chain atoms in helix G, whereas neither the homologous residue Phe 68, nor any other aromatic residue in the N-domain, shows such interactions with helix C (Fig. 3*a*).

Our study indicates that the C-terminal domain of apo calmodulin is considerably less stable than the N-terminal domain. Not only are the back-bone amide hydrogen exchange rates much faster in the C-terminal domain, but there is also a measurable population of at least one alternate conformation. This alternate conformer has a lifetime of several hundred microseconds[16] and, as a result of this short lifetime, it does not give rise to observable resonances.

It is interesting to note that trypsin digestion experiments show rapid cleavage at residue Arg 106 in

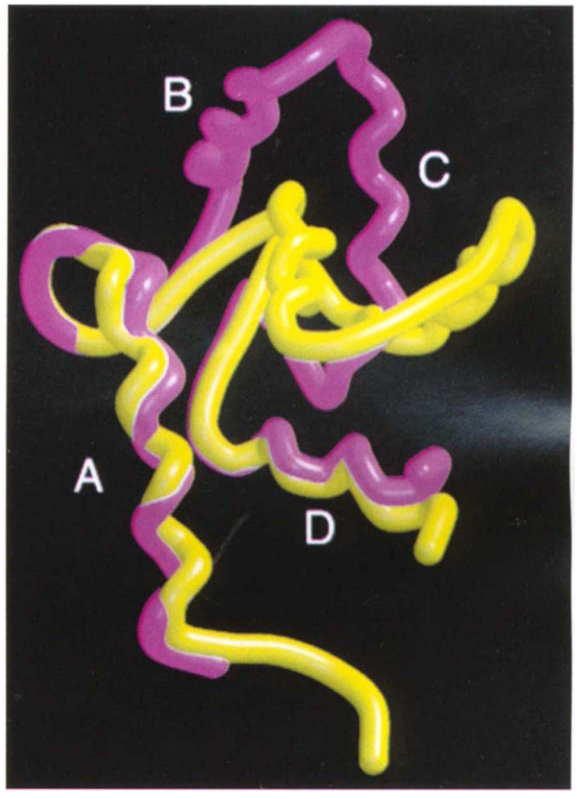

Fig. 6 Superposition of the N-terminal domain of apo calmodulin (yellow) with the X-ray structure of the N-terminal domain of Ca^{2+}-ligated calmodulin[2] (magenta).

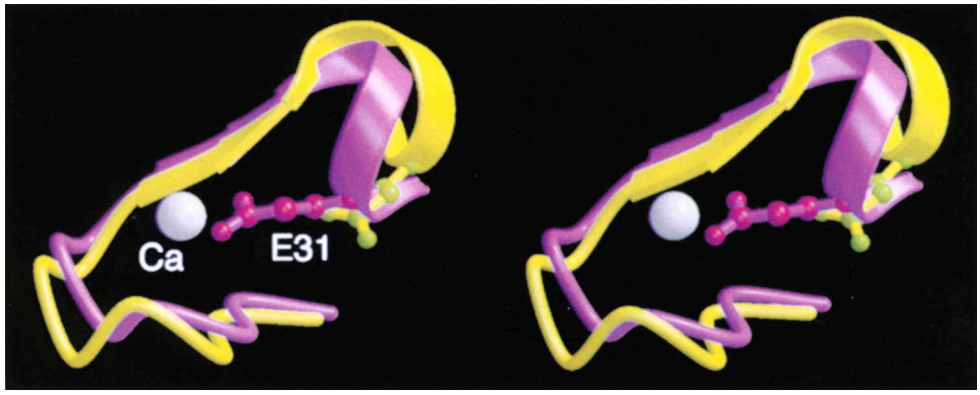

Fig. 7 Stereo view of the comparison of conformation of residues 20–31, constituting the first Ca^{2+}-binding site, in the apo (yellow) and in the Ca^{2+}-ligated state[2] (magenta). The calcium ion is shown in gray, the side-chain atoms of Glu 31 in green (apo) and red (Ca^{2+}-ligated). The back bones have been superimposed to yield a best fit for residues 20–27.

apo calmodulin[26], near the middle of helix F. The apo calmodulin back bone must have a non-helical structure in this region at least part of the time in order to be accessible to the active site of the protease. Based on these considerations, we propose that helix F is not formed in the minor conformer. Qualitatively, this also agrees with a microcalorimetry study[27], which indicated that the melting behavior in the absence of Ca^{2+} for the C-terminal domain is not compatible with that of a single, well-ordered structure

NMR structure *versus* model

The N-terminal domain of apo calmodulin closely resembles that of the Ca^{2+}-free N-terminal domain of troponin C (ref. 9) and that of the apo C structure (Table 2). The apparent disagreement between the orientation of helix D in the model and ^{15}N relaxation data recorded for apo calmodulin[16] is caused, in part, by the algorithm used for measuring the interhelical angles. Whereas Strynadka and James[8] reported a C/D interhelix angle of 151°, their model coordinates correspond to a C/D angle of only 141° when using the algorithm outlined in the footnote to Table 1. The C/D angle measured for the NMR apo calmodulin structure is somewhat smaller (130°) and the difference in the orientation of helices C and D is sufficiently large to explain their different ^{15}N relaxation behaviour.

The back bone of the N-terminal domain NMR structure and of the apo calmodulin model[8] are superimposed in Fig. 5 and differ by only 1.13 Å for the back-bone and 1.87 Å for all non-hydrogen atoms, including surface-exposed flexible side chains. For example, several of the details regarding the 3_{10} extensions of helix A and the pronounced kink at Glu 31 are virtually identical to features seen in Ca^{2+}-free troponin C, and predicted by the apo calmodulin model. The main differences between the model and our structure are found in the slightly smaller angle between helices C and D (130° *versus* 141°), and the side-chain orientations of Leu 18, Glu 31, Met 51, and Met 71. The packing of the five Phe side chains is virtually identical to what is observed in the NMR structure.

Considering that the spread of the calculated C-terminal domain NMR structures relative to their mean is rather large (0.64 Å for residues 82–146), the 2.1 Å pairwise r.m.s.d. for the back-bone atoms between the model[8] and the NMR structure indicates that the two are qualitatively similar. A relatively large number of significant differences in the packing of the hydrophobic residues is found however, including the position of four of the aromatic residues (Phe 89, Tyr 99, Tyr 138, and Phe 141). The start of the second Ca^{2+}-binding loop, including residues Asp 129–Asp 131, and in particular the position of the Ile 130 side chain, also differs significantly from the model of Strynadka and James.

The conformational switch

In apo calmodulin, sequential helix pairs in the N-terminal domain (A/B, B/C, C/D, D/A), and the corresponding pairs in the C-domain, on average make interhelix angles of ~130°. Thus, in the absence of calcium, each calmodulin domain consists of a strongly twisted but tightly packed bundle of four antiparallel α-helices. Upon binding of Ca^{2+}, most of the change occurs within each of the 'EF-hands'. As can be seen from Fig. 6, helices A and D remain in similar positions relative to one another, as do B and C, but the A/B and C/D interhelix angles decrease by nearly 50° (Table 1), and a similar decrease is seen for the two EF-hands in the C-terminal domain. The 'hinge' in this EF-hand rearrangement occurs at the end of the first β-strand in the first calcium-binding site, whereas in the second Ca^{2+}-binding site it occurs just prior to the β-strand. In the first Ca^{2+}-binding site of the N-terminal domain, the hinge includes a sharp kink in helix B at Glu 31, but such a kink is not observed in any of the other helices.

The structural rearrangement upon binding of Ca^{2+} results in a pronounced hydrophobic pocket on the surface of each domain, which is absent in apo calmodulin. The importance of these hydrophobic pockets was confirmed by the NMR and X-ray structures of calmodulin complexed with three different synthetic target peptides, where each of these two pockets is filled by a long hydrophobic amino-acid side chain of the peptide[11,12,28].

The increased back-bone dynamics in the Ca^{2+} binding 'loop' regions in apo calmodulin lowers the precision at which these structures can be determined. In addition, precision of the C-terminal domain is decreased by the conformational averaging process mentioned above.

For the second Ca^{2+}-binding site, multiple side-chain conformations observed for Val 55 and Ile 63 also decrease the precision of the structure in this region. Nevertheless, the back-bone atoms of residues 56–61 superimpose on those in the Ca^{2+}-ligated X-ray structure[2] with an r.m.s.d. of 0.50 Å, and residues 63–67 fit to within 0.22 Å.

Despite the increased amplitude of the back-bone dynamics, the average structure of the first Ca^{2+}-binding site

Table 3 Structural statistics and atomic r.m.s. differences[1]

a Structural statistics

	N-dom.(1–75)	C-dom.(76–148)
r.m.s.d. from experimental distance constraints (Å)[2]		
All (1122/733)[3]	0.040	0.079
Intraresidue ROE (209/174)	0.034	0.061
Intraresidue NOE (97/61)	0.021	0.087
Sequential ROE (|i - j| = 1) (203/189)	0.064	0.125[2]
Sequential NOE (|i - j| = 1) (47/21)	0.017	0.101
Medium range NOE/ROE (238/117)	0.032	0.057
Long range NOE/ROE (|i - j| > 5) (293/150)	0.020	0.087
H-bond (25/20)	0.010	0.018
r.m.s.d. from dihedral constraints (deg) (201/199)	0.09	0.30
Deviations from idealized covalent geometry		
Bonds (Å) (1157/1119)	0.0042	0.0061
Angles (deg) (2091/2011)	0.55	0.62
Impropers (deg) (574/568)	0.33	0.56
E_{L-J} (kcal mol^{-1})	-355	-293
E_{dihed} (kcal mol^{-1})	0.5	2.2
E_{NOE} (kcal mol^{-1})	74[2]	323[2]
E_{repel} (kcal mol^{-1})	43	109

b Atomic r.m.s. differences (Å)

	N-domain (5–75)		C-domain (82–146)	
	Back-bone atoms	All atoms	Back -bone atoms	All atoms
<SA> vs SA[1]	0.35	0.71	0.64	1.24

[1]Statistics are calculated over 25 simulated annealing structures, <SA>, selected on the basis of their lowest total energy; SA is the mean structure obtained by averaging the coordinates of the individual structures, best fitted to each other, including only residues 5–75 and 82–146. The refinement protocol and force constants were essentially identical to those reported by Qin *et al.*[43]

[2]Violations include N- and C-terminal residues where, for example, strong $d_{\alpha N}$ and d_{NN} NOEs result in distance constraints which can not be satisfied simultaneously by a single structure.

is reasonably well determined. As shown in Fig. 7, the back bone of the first eight residues (Asp 20–Ile 27) superimposes quite well upon the corresponding residues in the Ca^{2+}-ligated X-ray structure[2], with an r.m.s.d. of 0.55 Å (Fig.7). As expected, the side chains of Asp 22 and Asp 24 (not shown), involved in ligating Ca^{2+}, adopt different conformations. The back-bone atoms of the last four residues (Thr 28 through Glu 31) also superimpose well on the corresponding atoms in the X-ray structure (r.m.s.d.=0.21 Å). However, these four residues are rotated relative to the Ca^{2+}-ligated structure in such a way that the side-chain carboxyl oxygens of Glu 31, which constitute a bidentate ligand for Ca^{2+}, are several Å farther away from the position where Ca^{2+} is found in the Ca^{2+}-ligated structure (Fig. 7). Thus, this Ca^{2+}-binding site is partially pre-formed, requiring only rearrangement of two Asp side chains to coordinate Ca^{2+}, together with the back-bone carbonyl oxygen of Thr 26. However, coordination of the pivotal Glu 31 carboxyl oxygens requires a change in the back-bone conformation in this region, which triggers the dramatic structural rearrangement between the apo and the Ca^{2+}-ligated states.

Methods

Recombinant *Xenopus* calmodulin was overexpressed in *Escherichia coli* (strain AR58) containing the expression vector pTNco12. A total of four NMR samples was used in the present study, each at a concentration of 1–1.8 mM, 100 mM KCl, 1.5 mM EDTA, 100 µM sodium azide, pH 6.3. One sample contained 7.6 mg of uniformly ^{15}N-enriched calmodulin in 250µl 95% H_2O, 5% D_2O, using a Shigemi (Shigemi Inc., Allison Park, Pa.) microcell. Two samples of uniformly $^{13}C/^{15}N$ enriched calmodulin were prepared, one in 95% H_2O, one in 99.98% D_2O, each in a regular NMR sample tube. One 'reverse-labelled' sample, dissolved in 99.98% D_2O, was prepared, uniformly enriched in ^{13}C and ^{15}N, except for Phe which was at natural abundance[21]. All NMR experiments were conducted at 23 °C, using a Bruker AMX-600 spectrometer equipped with a triple resonance probehead and pulsed field gradients. Spectra were processed using the software package NMRPipe[29] and analyzed using the programs PIPP and CAPP[30].

Resonance assignments were obtained primarily on the basis of CBCA(CO)NH and CBCANH experiments[31] conducted in H_2O, and HCCH-TOCSY experiments[32] carried out on the D_2O sample of uniformly enriched protein. Resonance assignments of the Phe aromatic protons were obtained from ^{12}C-filtered NOESY and HOHAHA spectra on the reverse-labelled sample, using procedures described previously[21]. Methionine methyl groups were assigned by *J*-correlation with the intraresidue H^{γ}, C^{β} and C^{γ} (ref. 33).

Proton-proton distance restraints involving exchangeable protons were obtained from a 25-ms mixing period 3D water-flip-back ^{15}N-separated ROESY[34], using a 4D gradient-enhanced[35] $^{15}N/^{13}C$-separated NOESY as a guide to facilitate the assignment of the 3D spectrum. Distance constraints involving non-exchangeable aliphatic protons and Tyr residues were obtained from a 4D $^{13}C/^{13}C$ separated NOESY spectrum[36]. Intra- and interresidue distance restraints involving Phe residues were obtained from a ^{12}C double-half-filtered 2D NOESY spectrum using the reverse-labeled sample, and distance restraints between Phe protons and other types of residues were obtained from ^{13}C-separated, ^{12}C-filtered 3D NOESY. All NOESY spectra were recorded with an 80 ms mixing period. For NOEs to non-stereospecifically assigned protons, methyl protons, or aromatic Phe protons with identical chemical shifts, constraints were entered in the X-PLOR program[37] by summation[38] ($r^{-6}=r_1^{-6}+r_2^{-6}$). For NOE-derived distance constraints involving pairs of stereospecifically assigned methylene protons, which invariably show similar cross-peak patterns due to rapid spin diffusion, weak cross-peaks were not converted to distance constraints if the geminal proton showed a significantly stronger NOE cross-peak to the same proton.

Quantitative *J*-correlation experiments[39] yielded 133 $^3J(H^NH^{\alpha})$, 150 $^3J(NH^{\beta})$, 135 $^3J(C'H^{\beta})$, 141 $^3J(H^{\alpha}H^{\beta})$, 25 $^3J(H^{\alpha}N)$, 26 $^3J(C^{\beta}C^{\alpha})$, 31 $^3J(C^{\gamma}C')$, 30 $^3J(C^{\gamma}N)$, and 63 $^3J(C^{methyl}H)$ couplings. These numbers include cases (~40%) where the absence of a cross-peak provided a useful upper limit for the size of the *J*-coupling. For the back-bone angles ϕ and ψ, the *J*-couplings were converted to loose angular constraints (ϕ=60° ± 20° for $^3J(H^NH^{\alpha})$ < 5.5 Hz; ϕ=120° ± 25° for $^3J(H^NH^{\alpha})$ > 8 Hz; ψ=-60° ± 40° for $^3J(H^{\alpha}N)$ > 1.5 Hz). For the side-chain angles, χ_1 and χ_2, constraints were only used if all *J*-couplings and the ROE patterns were consistent with a single rotameric state. Constraints for these angles were entered as the ideal rotamer (±60° or 180°) values with a tolerance of 20° to 40°, depending on how close the *J*-values were to the ideal rotamer values.

One hundred structures were calculated using the hybrid distance geometry and simulated annealing protocol[40], implemented using the program *X-PLOR 3.1* (ref. 37). A target

function using quadratic harmonic potential terms for covalent geometry, square-well quadratic potentials for experimental distance and dihedral constraints, and a quartic van der Waals repulsion term for non-bonded contacts, was minimized during the simulated annealing phase of the protocol. Of these, the 25 lowest energy structures were chosen and subjected to an additional simulated annealing and refinement phase. Analysis of the structure with the program PROCHECK[41] indicates that the N-terminal domain is of high quality, with 92% of the residues evaluated as being within the most favored region of the Ramachandran map. The C-terminal domain scores lower (80%), which reflects the extensive conformational averaging and the presence of mutually exclusive constraints, particularly in the highly flexible linker region (Met 76 through Glu 82) and near the C-terminus (Thr 146–Lys 148). Coordinates for apo-calmodulin have been deposited with the Brookhaven Protein Data Bank (ident. code 1CFC).

Received 17 May; accepted 20 July 1995.

Acknowledgements
We thank G.M. Clore for many useful comments and suggestions, J. Kuszewski for assistance with the X-PLOR program, and D. Garrett for assistance with the programs PIPP and CAPP. Coordinates of the apo calmodulin model[8] were kindly provided to us by N.C.J. Strynadka. This work was supported by the AIDS Targeted Anti-Viral Program of the Office of the Director of the National Institutes of Health.

1. *Molecular aspects of cellular regulation* Cohen, P. & Klee, C.B. eds. (Elsevier, Amsterdam, 1988).
2. Babu, Y.S., Bugg, C.E. & Cook, W.J. Structure of calmodulin refined at 2.2 Å resolution. *J. molec. Biol.* **204**, 191–204 (1988).
3. Barbato, G., Ikura, M., Kay, L.E. & Bax, A. Backbone dynamics of calmodulin studied by ^{15}N relaxation using inverse detected two-dimensional NMR spectroscopy: The central helix is flexible. *Biochemistry* **31**, 5269–5278 (1992).
4. Heidorn, D.B. & Trewhella, J. Comparison of the crystal and solution structures of calmodulin and troponin-C. *Biochemistry* **27**, 909–915 (1988).
5. Seeholzer, S.H. & Wand, A.J. Structural characterization of the interactions between calmodulin and skeletal muscle myosin light chain kinase: Effect of peptide (576-594)G binding on the Ca^{2+}-binding domains. *Biochemistry* **25**, 4011–4020 (1989).
6. Ikura, M., Kay, L.E. & Bax, A. A novel approach for sequential assignment of ^{1}H, ^{13}C, and ^{15}N spectra of larger proteins: Heteronuclear triple-resonance NMR spectroscopy. Application to calmodulin. *Biochemistry* **29**, 4659–4667 (1990).
7. Kretsinger, R.H. Structure and evolution of calcium-modulated proteins. *CRC crit. rev. Biochem.* **8**, 119–174 (1980).
8. Strynadka, N.C.J. & James, M.N.G. Two trifluoroperazine-binding sites on calmodulin predicted from comparative molecular modeling with troponin-C. *Proteins Struct. Funct. Genet.* **3**, 1–17 (1988).
9. Herzberg, O. & James, M.N.G. Refined crystal structure of troponin-C from turkey skeletal muscle at 2.0 Å resolution. *J. molec. Biol.* **203**, 761–779 (1988).
10. Herzberg, O., Moult, J., & James, M.N.G. A model for the Ca^{2+}-induced conformational transition of troponin-C. *J. biol. Chem.* **261**, 2638–2644 (1986).
11. Ikura, M. *et al.* Solution structure of a calmodulin-target peptide complex by multi-dimensional NMR. *Science* **256**, 632–638 (1992).
12. Meador, W.E., Means, A.R. & Quiocho, F.A. Target enzyme recognition by calmodulin: 2.4 Å structure of a calmodulin-peptide complex. *Science* **257**, 1251–1255 (1992).
13. Skelton, N.J., Kördel, J., Akke, M., Forsen, S., & Chazin, W.J. Signal transduction versus buffering activity in Ca^{2+}-binding proteins. *Nature struct. Biol.* **1**, 239–245 (1994).
14. Gagné, S.M. *et al.* Quantification of the calcium-induced secondary structural changes in the regulatory domain of troponin-C. *Prot. Sci.* **3**, 1961–1974 (1994).
15. Finn, B.E., Drakenberg, T. & Forsen, S. The structure of apo-calmodulin: A ^{1}H NMR examination of the carboxy-terminal domain. *FEBS Lett.* **336**, 368–374 (1994).
16. Tjandra, N., Kuboniwa, H., Ren, H. & Bax, A. Rotational dynamics of calcium-free calmodulin studied by ^{15}N NMR relaxation measurements. *Eur. J. Biochem.* **230**, 1014–1024 (1995).
17. Bax, A., Max, D. & Zax, D. Measurement of multiple-bond ^{13}C-^{13}C *J*-couplings in a 20-kDa protein-peptide complex. *J. Am. chem. Soc.* **114**, 6923–6925 (1992).
18. Bothner-By, A.A. *et al.* Structure determination of a tetrasaccharide: Transient nuclear Overhauser effects in the rotating frame. *J. Am. chem. Soc.* **106**, 811–813 (1984).
19. Bax, A., Sklenar, V. & Summers, M.F. Direct identification of relayed nuclear Overhauser effects. *J. magn. Reson.* **70**, 327–331 (1986).
20. Vuister, G.W. *et al.* Solution structure of the DNA-binding domain of *Drosophila* heat shock transcription factor. *Nature struct. Biol.* **1**, 605–614 (1994).
21. Vuister, G.W., Kim, S.-J., Wu, C. & Bax, A. 2D and 3D NMR study of phenylalanine residues in proteins by reverse isotopic labeling. *J. Am. chem. Soc.* **116**, 9206–9210 (1994).
22. Akke, M., Skelton, N.J., Kördel, J., Palmer, A.G. & Chazin, W.J. Effects of ion binding on the backbone dynamics of calbindin D_{9k} determined by ^{15}N NMR relaxation. *Biochemistry* **32**, 9832–9844 (1993).
23. Wüthrich, K. *NMR of proteins and nucleic acids* (Wiley, New York, 1986).
24. Gronenborn, A.M. & Clore, G.M. Identification of N-terminal helix capping boxes by means of ^{13}C chemical shifts. *J. biomol. NMR* **4**, 455–458 (1994).
25. Seale, J.W., Srinivasan, R. & Rose, G.D. Sequence determinants of the capping box, a stabilizing motif at the N-termini of α-helices. *Prot. Science* **3**, 1741–1745 (1994).
26. Newton, D.L., Oldewurtel, M.D., Krinks, M.H., Shiloach, J. & Klee, C.B. Agonist and antagonist properties of calmodulin fragments. *J. biol. Chem.* **259**, 4419–4426 (1984).
27. Tsalkova, T.N. & Privalov, P.L. Thermodynamic Study of domain organization in troponin-C and calmodulin. *J. molec. Biol.* **181**, 533–544 (1985).
28. Meador, W.E., Means, A.R. & Quiocho, F.A. Modulation of calmodulin plasticity in molecular recognition based on X-ray structures. *Nature* **262**, 1718–1721 (1993).
29. Delaglio, F. *et al.* NMRPipe: a multidimensional spectral processing system based on UNIX pipes. *J. biomol. NMR* **in the press**.
30. Garrett, D.S., Powers, R., Gronenborn, A.M., and Clore, G.M. A common sense approach to peak picking in two-, three-, and four-dimensional spectra using automatic computer analysis of contour diagrams. *J. magn. Reson.* **95**, 214–220 (1991).
31. Grzesiek, S. & Bax, A. Amino acid type determination in the sequential assignment procedure of uniformly ^{13}C/^{15}N enriched proteins. *J. biomol. NMR* **3**, 185–204 (1993).
32. Bax, A., Clore G.M. & Gronenborn, A.M. ^{1}H-^{1}H correlation via isotropic mixing of ^{13}C magnetization: A new three-dimensional approach for assigning ^{1}H and ^{13}C spectra of ^{13}C-enriched proteins. *J. magn. Reson.* **88**, 425–431 (1990).
33. Bax, A., Delaglio, F., Grzesiek, S. & Vuister, G.W. Resonance assignment of methionine methyl groups and χ_3 angular information from long range proton-carbon *J*-correlation in a calmodulin-peptide complex. *J. biomol. NMR* **4**, 787–797 (1994).
34. Grzesiek, S.& Bax, A. Measurement of amide proton exchange rates and NOE with water in ^{13}C/^{15}N enriched calcineurin B. *J. biomol. NMR* **3**, 627–638 (1993).
35. Muhandiram, D.R., Xu, G.Y. & Kay, L.E. An enhanced-sensitivity pure absorption gradient 4D ^{13}C-edited NOESY experiment. *J. biomol. NMR* **3**, 463–470 (1993).
36. Vuister, G.W. *et al.* Increased resolution and improved spectral quality in four-dimensional ^{13}C/^{13}C separated HMQC-NOESY-HMQC spectra using pulsed field gradients. *J. magn. Reson.* **B 101**, 210–213 (1993).
37. Brünger, A.T. *X-PLOR Version 3.1: A System for X-ray Crystallography and NMR*, Yale University, New Haven, CT, USA (1992).
38. Nilges, M. A calculation strategy for the structure determination of symmetric dimers by ^{1}H NMR. *Proteins Struct. Funct. Genet.* **17**, 297–309 (1993).
39. Bax, A. *et al.* Measurement of homo- and heteronuclear *J*-couplings from quantitative *J*- correlation. *Meth. Enzymol.* **239**, 79–125 (1994).
40. Nilges, M., Clore, G. M. & Gronenborn, A. M. Determination of three-dimensional structures of proteins from interproton distance data by hybrid distance geometry-dynamical simulated annealing calculations. *FEBS Lett.* **229**, 317–324 (1988).
41. Laskowski, R.A., MacArthur, M.W., Moss, D.S. & Thornton, J. PROCHECK: a program to check the stereochemical quality of protein structures. *J. appl. Crystallogr.* **26**, 283–291 (1993).
42. Kraulis, P.J. MOLSCRIPT: a program to produce detailed and schematic plots of protein structures. *J. appl. Crystallogr.* **24**, 946–950 (1991).
43. Qin, J., Clore, G.M. & Gronenborn, A.M. The high-resolution three-dimensional solution structures of the oxidized and reduced states of human thioredoxin. *Structure* **2**, 503–522 (1994).